Combustion and Flame 173 (2016) 187–194

Contents lists available at ScienceDirect

Combustion and Flame

journal homepage: www.elsevier.com/locate/combustflame

Kinetic studies of ozone assisted low temperature oxidation of dimethyl ether in a flow reactor using molecular-beam mass spectrometry

Hao Zhao*, Xueliang Yang, Yiguang Ju

Department of Mechanical and Aerospace Engineering, Princeton University, Princeton, NJ 08544, USA

ARTICLE INFO

Article history:
Received 17 May 2016
Revised 14 June 2016
Accepted 12 August 2016
Available online 12 September 2016

Keywords:
DME
Low temperature chemistry
Ozone assisted oxidation
Flow reactor
Molecular beam mass spectrometry

ABSTRACT

The ozone assisted low temperature oxidation chemistry of dimethyl ether (DME) from 400 K to 750 K has been investigated in the mixture of DME/O_3/O_2/He/Ar in an atmospheric-pressure flow reactor coupled with the molecular beam mass spectrometry (MBMS) sampling technique. The mole fraction of ozone was varied from 0 to 0.146% in the mixture to study its enhanced kinetic effect on DME oxidation. The mole fractions of DME, O_2, O_3, CH_2O, H_2O_2, CO, CO_2, and CH_3OCHO were quantified as functions of temperature at a fixed total volumetric flow rate. The experimental results revealed that the presence of ozone dramatically enhances the low temperature DME oxidation. Numerical simulations using the existing kinetic models (Kurimoto's model (KM) (Kurimoto et al., 2015), Burke's model (BM) (Burke et al., 2015), and Wang's model (WM) (Wang et al., 2015)) with an ozone sub-mechanism over-predicted the DME oxidation significantly. The observed large discrepancies between models and experiments for DME, CH_2O, O_2 and CH_3OCHO mole fractions suggested that there were large uncertainties in the branching ratios of two competing chain-propagation and chain-branching reaction pairs involving $CH_3OCH_2O_2$ and $CH_2OCH_2O_2H$ radicals at low temperature.

1. Introduction

Dimethyl ether (DME) has been widely investigated as an alternative fuel in diesel and HCCI engines due to many merits [1,2].As one of the simplest fuels exhibiting two-stage oxidation behaviors, it has been widely used as a model fuel to study the low temperature oxidation mechanism [3,4] and cool flames [5,6].

Several DME mechanisms that describe the oxidation of DME have been developed [4,7–9] based on experimental studies of DME ignition delays [10], jet stirred reactors (JSR) [11,12] and flow reactors [3,4,7], and low and high pressure flames [13,14]. However, recent flow reactor [4,7] and JSR [15] experiments have shown that all these mechanisms could possibly over-predict DME consumption and HO_2 and H_2O_2 formation in the low temperature [3,16]. More recently, Kurimoto et al. [4] investigated the low and intermediate temperature oxidation of DME using molecular beam mass spectrometry (MBMS) and Faraday rotation spectroscopy and found that all the important intermediate species such as HO_2, H_2O_2, CH_2O, CO, and CH_3OCHO were significantly over-predicted. Detailed analysis revealed that the branching ratio, $CH_2OCH_2O_2H$ dissociation to its association with O_2, was the main cause of the large discrepancies. A factor of 3–4 increase of the $CH_2OCH_2O_2H$ dissociation rate to CH_2O formation was found to results in much improved agreement between measured and predicted distributions of CO, CH_2O, H_2O_2 and HO_2. Similar intermediates over-predictions were also reported in [16]. Unfortunately, the consumption of DME at atmospheric pressure is very small, and the measurement uncertainty is large, limiting the model prediction [4]. Moreover, in practical combustion in engines, the exhaust gas recirculation (EGR) and turbulent mixing could introduce O and OH radical productions through NO_2 decomposition and NO*x* reactions with HO_2, and thus might significantly enhance the low temperature reactivity of fuels [17]. Therefore, to achieve a better understanding of the low temperature mechanism of DME involving initial radicals, it is necessary to investigate the effects of radical sensitized DME's kinetics at low temperatures with simple chemistry couplings.

Recently, it was found that self-sustaining cool flames could be observed in a very short timescale (a few milliseconds) for DME with ozone sensitization [6,18]. However, the simulations of cool flames showed that the kinetic model of DME over-predicted the cool flame temperature and CO_2 formation. Unfortunately, few kinetic studies of low temperature fuel oxidation with ozone sensitization or radical addition were reported in the literature.

* Corresponding author.
E-mail address: haozhao@princeton.edu (H. Zhao).

http://dx.doi.org/10.1016/j.combustflame.2016.08.008
0010-2180/

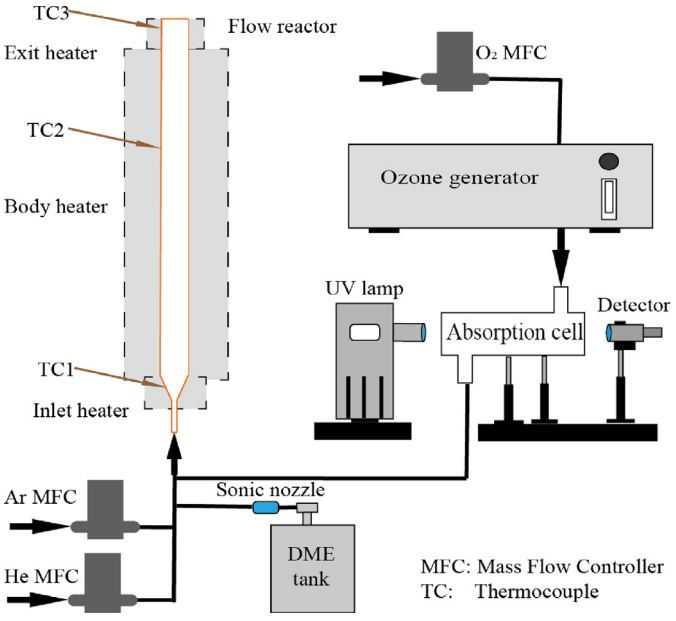

Fig. 1. Schematic of the flow reactor and ozone generation system.

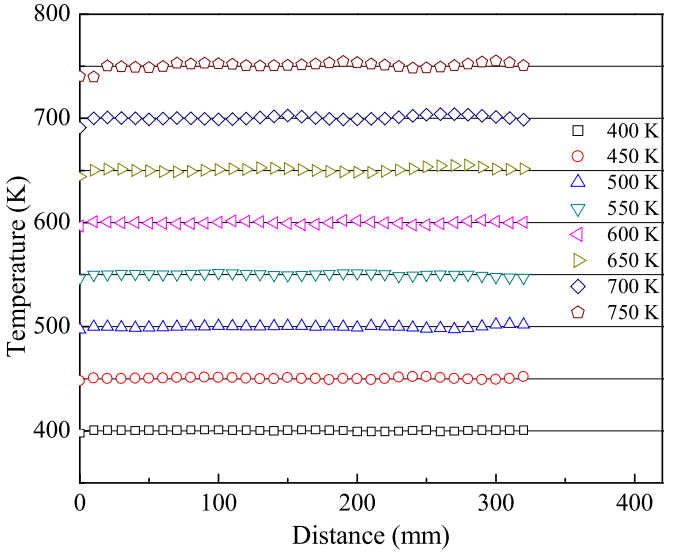

Fig. 2. Temperature profiles of the flow reactor from 400 to 750 K. The distances of 0 and 320 mm are referred, respectively, to the inlet and exit of the reactor body. Maximum of ±4 K deviation from the setting temperature was observed in the inlet of 750 K experiments.

In this paper, we report experiments of ozone assisted low temperature oxidation of DME in an atmospheric-pressure flow reactor using the molecular beam mass spectrometry sampling technique to identify the major low temperature reaction pathways by quantitatively measuring DME, O_2, O_3, CH_2O, H_2O_2, CO, CO_2, and CH_3OCHO over a temperature range from 400 to 750 K. The mole fraction of ozone was varied from 0 to 0.146%. The experimental results were compared with model predictions by using three recently developed/updated DME mechanisms with an ozone sub-mechanism. The reaction path analysis and sensitivity analyses were performed to identify the important reactions corresponding to the reactants consumption and products formation. Comparisons between model predictions and experiments were made to identify the uncertainties in the branching ratios of the competing chain propagating and branching reaction pairs of key radicals.

2. Experimental methods and kinetic models

2.1. Flow reactor

All the experiments were performed in a newly designed atmospheric-pressure flow reactor coupled with an MBMS system and the details of MBMS have been reported in [3].

The schematic of the flow reactor configuration is shown in Fig. 1. The laminar flow reactor was a cylindrical quartz tube of 17 mm inner diameter, 320 mm in length. The nozzle is designed to have no recirculation zone with the Reynolds number around O(1), according to the previous modeling using OpenFoam [4]. Reactants were supplied through an inlet channel of 100 mm length and 2 mm inner diameter. The quartz tube was jacketed within a stainless steel sleeve, and this assembly was placed inside a tube furnace [3]. DME was supplied by a sonic nozzle and the volumetric flow rates of Ar, He, and O_2 were regulated by mass flow controllers (MKS, 0.5% uncertainty). To improve the temperature distribution at the exit and keep a uniform temperature profile throughout the reactor, a 3-stage heating arrangement was employed in the present study. The measured temperature distributions inside the reactor at different pre-specified temperatures are shown in Fig. 2. It is seen that the maximum temperature fluctuation of the temperature profile is less than ±4 K throughout the tube body.

2.2. Ozone generation and UV absorption spectroscopy measurement

In the experiments, ozone was produced by an ozone generator (Ozone Solutions, TG-20) from a pure oxygen stream and mixed with other gases downstream (Fig. 1) at room temperature. The ozone mole fraction in the mixture was measured in an UV absorption cell using a Deuterium lamp (Oriel) and a spectrometer with a charged couple device (CCD) detector (Ocean Optics, USB 2000+). The detailed procedure has been described in [19,20]. The absorption spectra from 260 to 280 nm were used to extract the mole fraction. O_3 mole fraction was measured, respectively, right after the ozone generator and at the inlet and the outlet of the flow reactor at room temperature (293 K) with fixed flow conditions using the optical absorption method. The relative change of O_3 mole fractions was less than 2%. MBMS measurement of O_3 mole fraction also confirmed this result. Thus, there is no significant decomposition of O_3 in the gas line and flow reactor at room temperature.

2.3. Molecular beam mass spectrometer

An electron-ionization MBMS was employed to measure DME, O_2, O_3, CO, CO_2, H_2O_2, CH_2O, and CH_3OCHO at the exit of the flow reactor. The mass resolution of the MBMS was typically around 850. Each important species was calibrated directly by flowing the mixture with known mole fraction in excessive Helium. In the experiments, Argon was fixed at 2% in all mixtures and the relative intensity of each species to Argon reflected the mole fraction in the mixture comparing to the signals of calibration mixtures. Oxygenated species (H_2O_2, CH_2O, and CH_3OCHO) were calibrated using the mixtures prepared in a quartz vaporizer with coflow of heated Helium and Argon. A syringe pump (Harvard Apparatus, PHD 22/2000) was used to regulate the flow rates of these liquid samples (H_2O_2 30 wt% in water solution, CH_2O 37 wt% in water solution, CH_3OCHO liquid). Details of the species calibration were described elsewhere [3,4,14].

The measurement has a maximum uncertainty of 20%, which is mainly from the direct species calibration for MBMS, the electron impact (20 eV ±1 eV) in MBMS, and the O_3 measurement using the UV adsorption method. For gas phase species (DME, O_2, CO, CO_2,

Table 1
Experimental conditions.

Case	% DME	%O_2	%O_3	%Ar	%He	Flow rate (L/min)	Residence time (s)	Temperature range (K)
1	0.400	3.654	0.146	2.000	93.800	7.5	0.45–0.24	400–750
2	0.400	3.762	0.072	2.000	93.770	7.5	0.45–0.24	400–750
3	0.400	3.870	0.000	2.000	93.730	7.5	0.45–0.24	400–750

and O_3) calibrations, the uncertainty is around 10%; while for liquid samples calibrations (CH_2O, H_2O_2, and CH_3OCHO), the data has an uncertainty of 20%.

For O_3 in MBMS, it has two reactions, $O_3 + e = O_3^+ + 2e$, $O_3 + e = O + O_2^+ + 2e$ or $O^+ + O_2 + 2e$. If ionization energy is too large, most of O_3 will be fragment to O_2 and O, however, if it is too small, signal will be too small to be observed. Thus, we chose 20 eV as a trade-off. The limiting detection intensity of a specific species in the intensity-flight time diagram is around O(10), while the intensity of O_3 signal is O(100) at ionization energy of 20 eV. Experiments showed that significant O_3^+ exists in the system.

2.4. Experimental conditions

The experimental conditions used in this study are listed in Table 1.

2.5. Kinetic models and simulation methods

Three recently developed/updated DME mechanisms, Kurimoto's model (KM) [4], Burke's model (BM) [8], and Wang's model (WM) [21], were coupled with Princeton O_3 sub-mechanism. The O_3 sub-mechanism was attached in the supplementary material, in which the O_3 decomposition reaction and O_3 reactions with O, H, OH, HO_2, H_2O, CO, HCO, and CH_3 were considered. As to the flow field of the laminar flow reactor, Dryer et al., discussed the multi-dimensional effect of flow reactor in the paper [22]. This effect was investigated in our previous paper [4], in which the simulation using 0-D module in Chemkin [23] was in comparison with the 2-D module in OpenFoam. The simulated mole fractions of DME, O_3, CO_2, and CH_2O using 0-D and 2-D modules were also compared at 600 K in Fig. S2 in the supplementary material of this paper, and the species mole fraction discrepancies between these two modules were less than 10%. Additionally, the characteristic time of species radial diffusion (0.1–0.2 s) is less than the residence time (~0.5 s) under these experimental conditions, keeping a nearly uniform species distribution in the radial direction of the flow reactor; on the other hand, the axial species diffusion time scale is much larger than the residence time, which meets the negligible axial diffusion assumption in flow reactors. Taking O radical as an example, the radial diffusion characteristic time is around 0.15 s, which is less than the residence time (~0.5 s), while the axial diffusion time is 212 s, which meets the flow reactor assumption. Thus, the laminar flow reactor could be modeled by using the plug flow model (0-D) in Chemkin from 400 K to 750 K.

3. Results and discussion

Figure 3 depicts the measured mole fraction of DME versus the gas temperature of the flow reactor under different ozone addition levels (Table 1). It is seen that without ozone addition, very little DME is oxidized through all the experimental temperature range. However, when 0.072% or 0.146% of ozone is added to the mixture in the experiment (cases 1 and 2), significant oxidation of DME is observed from 450 K. Moreover, an increase of ozone mole fraction leads to higher consumption of DME (36.4% at 600 K for case 1and 24.9% for case 2). Above 600 K, the reaction rate becomes slower,

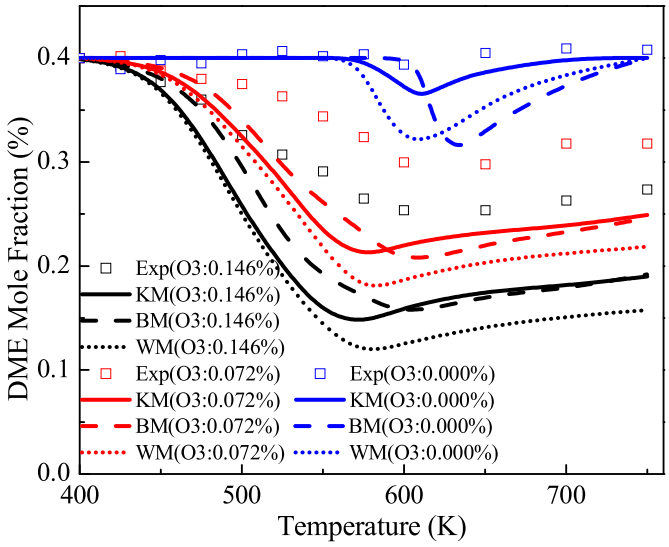

Fig. 3. DME mole fraction profiles with varied temperatures.

showing the typical negative temperature coefficient (NTC) behavior. It is clearly seen that not only DME oxidation increases significantly with ozone addition, but also the DME oxidation window is shifted a lower temperature down to 450 K. This result is very different from previous reports by Kurimoto et al. [4] and Herrmann et al. [12] in which no significant DME oxidation was observed below 525 K without ozone addition. In addition, compared with experiment, DME oxidation is over-predicted in the simulation.

Actually, for the combustion kinetics investigation, the uncertainty may come from the experiment, the modeling method, and the kinetic mechanism. As is mentioned above, the uncertainty of this MBMS experiment is around 20%, which is typical for MBMS experiments. As to the 0-D homogeneous modeling, it has less than 10% difference compared with the 2-D modeling using OpenFoam. These uncertainties are acceptable, while the uncertainty from kinetics mechanism could be much larger, which comes, respectively, from four sources: (1) low temperature DME kinetics; (2) O_3 decomposition rate; (3) O radical (the most sensitive radical in this investigation) wall quenching; (4) the coupled reactions between O_3 and DME and other intermediates in low temperature.

As to the uncertainty from (2), O_3 decomposition experiment without DME addition (0.000%DME/3.654%O_2/0.146%O_3/2.000%Ar/94.200%He) was conducted with varied temperatures to investigate the uncertainty of O_3 decomposition reaction (Fig. 4). The uncertainty of ozone decomposition rate is around 20% from the literature [24]. It is seen that the experimental O_3 decomposition profile is well predicted by Princeton O_3 sub-mechanism. Therefore, it rules out the possibility that the uncertainty of O_3 decomposition rates is the major cause of the discrepancies of species profiles between experiments and simulations.

As to uncertainty from (3), the uncertainty of DME consumption in experiments may be also from O radical's quenching on the inner surface of the flow reactor via radial diffusion. The volumetric quenching of O radical through three body reaction is negligible

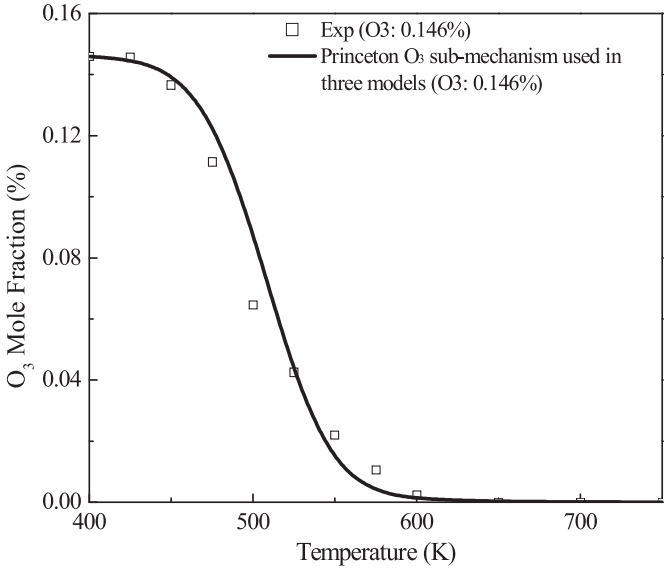

Fig. 4. O_3 mole fraction profiles with varied temperatures in the O_3 decomposition experiment.

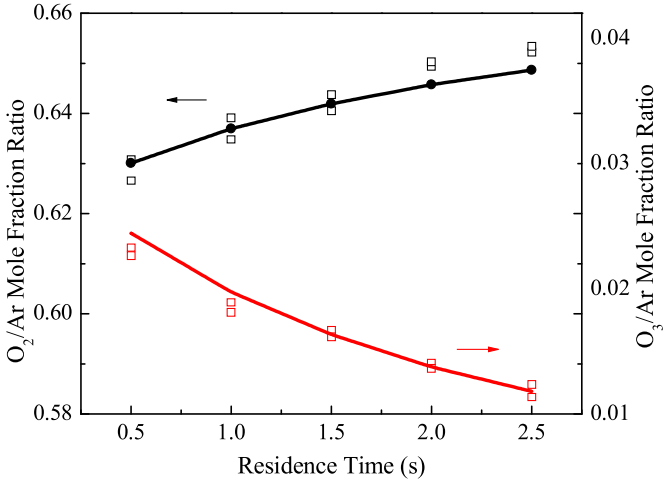

Fig. 5. O_2/Ar and O_3/Ar mole fraction ratio profiles with varied residence times. Symbols: experiment data; lines: simulation data using Princeton O_3 sub-mechanism.

because of low mole fraction of O radicals. With a higher quenching rate, the radical pool gets smaller and less DME is oxidized in the experiment. Note that the radical quenching via radial diffusion on the wall must be affected by the ratio of the characteristic times between radial diffusion and reaction (flow residence). To analyze O radical's quenching effect in this experiment, an O_3 decomposition experiment without DME addition was conducted with varied residence times (0.5–2.5 s) at 475 K. The residence time was chosen that reaction time scale was varied from comparable to longer time scales than the diffusion time scale so that the wall quenching effect, if any, could be observed. The residence time was adjusted by changing the flow rate of dilute gas, while the O_2 and Ar flow rates were fixed at 0.02 and 0.03 SLM, respectively. By fixing the power of the O_3 generator, the O_3 flow was also fixed in the reactants mixture. The characteristic reaction time of O_3 decomposition is around 3 s at 475 K, which is comparable with the convection time (0.5–2.5 s), and the O radical's characteristic diffusion time in the radial direction is around 0.15 s. From Fig. 5, the experimental O_2 and O_3 profiles with varied residence times are well predicted by Princeton O_3 sub-mechanism. O_2/Ar mole fraction ratio increases with residence time, while O_3/Ar mole fraction ratio decreases. With increasing the residence time, more O_3 molecules are decomposed, causing an increase of O_2 mole fraction. In the 0-D simulation, radical quenching is not considered. The good agreement between experimental data and simulation results of O_2 mole fraction indicates the O radical's quenching is negligible in the residence timescales above. For other radicals, like H and OH, their quenching effects on DME oxidation are less significant than O radical, which will be discussed in the sensitivity analysis part. Moreover, the estimated maximum mole fractions of H and OH are both around $O(10^{-8})$ at 600 K in the simulation, while it is around $O(10^{-7})$ for O radical. Thus, for other radicals, the wall quenching effect is less significant than O radical.

For the uncertainty from (4), there are coupled reactions between O_3 and DME and other intermediates in the reactive temperature range 500–650 K. The O_3 decomposition rate is $\sim O(10^6)$ [cm^3/(mol s)] at 600 K [24], while the rate of $CH_2O + O_3$ is $\sim O(10^3)$ [cm^3/(mol s)] at 600 K [25]. There is no existing rate for DME + O_3, and thus, the rate of $C_3H_8 + O_3$ is used to estimate the rate of DME + O_3, which is $\sim O(10^4)$ [cm^3/(mol s)] at 600 K [26]. Both of DME + O_3 and $C_3H_8 + O_3$ are considered as H abstraction reactions, and we could make the first order estimation of these two rates from the C–H bond energies and the number of sites of H abstraction. The C–H bond energy of DME is around 96.1 kcal/mol [27], while the energies of the two types C–H bonds in C_3H_8 are 98 and 96 kcal/mol, respectively [28]. The similar C–H bond energies of DME and C_3H_8 and the small change in the number of H abstraction site imply that the reaction rates of DME + O_3 and $C_3H_8 + O_3$ should be in the same order. The rate profiles (Fig. S1) with temperature are attached in the supplemental material as a reference. For O_3 reactions with other intermediates, because of the low mole fractions of intermediates, the rates are much lower. Thus, the O_3 decomposition reaction is much faster than O_3 reactions with other species. In summary, the discrepancy observed in the present experiment is mainly from DME's kinetics instead of the processes in (2), (3), and (4).

As to DME's kinetics, the reactivity of low temperature oxidation of DME is very sensitive to the consumption of $CH_2OCH_2O_2H$ [4]. There is a competing chain-propagation and chain-branching pair ((R1) and (R2)) associated with the consumption of $CH_2OCH_2O_2H$:

$$CH_2OCH_2O_2H = 2CH_2O + OH \quad (R_1)$$

$$CH_2OCH_2O_2H + O_2 = O_2CH_2OCH_2O_2H \quad (R_2)$$

(R1) is a chain-propagation reaction for one OH formation, and $O_2CH_2OCH_2O_2H$, produced from (R2), will decompose to form two OH radicals through the chain-branching channel. Therefore, the low temperature reactivity of DME is governed more by the consumption of $CH_2OCH_2O_2H$ through (R2) than through (R1). However, when temperature is above 600 K, (R1) becomes faster and more important than (R2) in consumption of $CH_2OCH_2O_2H$, resulting in less OH release and slower reactivity. As such, formaldehyde formation from (R1) is an important indicator of the system reactivity, which will be discussed below in more details. All of the three models show over-predictions of DME consumption. One possible reason for the over-predicted DME consumption is that the branching ratio of competing chain propagating and branching reaction pairs, (R1) and (R2), is too low at low temperature, resulting in the high reactivity of the system via (R2). Specifically, the chain branching ratio of (R1) and (R2) is defined as β_1 = net production of CH_2O from $CH_2OCH_2O_2H$/total consumption of $CH_2OCH_2O_2H$.

The measured O_2 profile is shown in Fig. 6. It is interesting to note that, different from DME, O_2 consumption is considerably

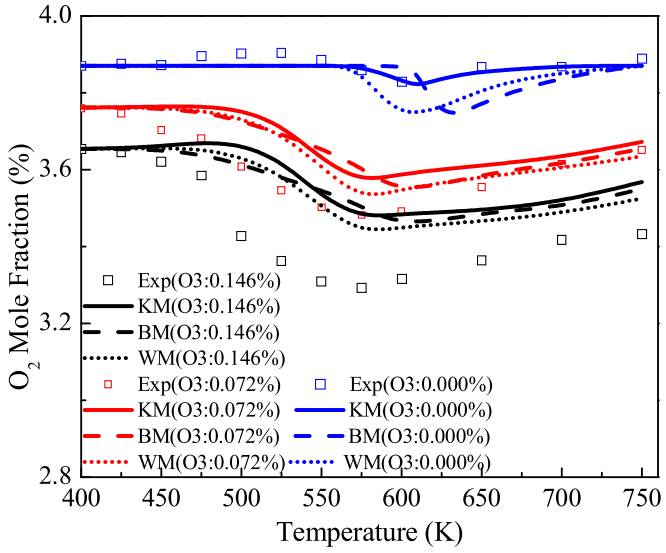

Fig. 6. O_2 mole fraction profiles with varied temperatures.

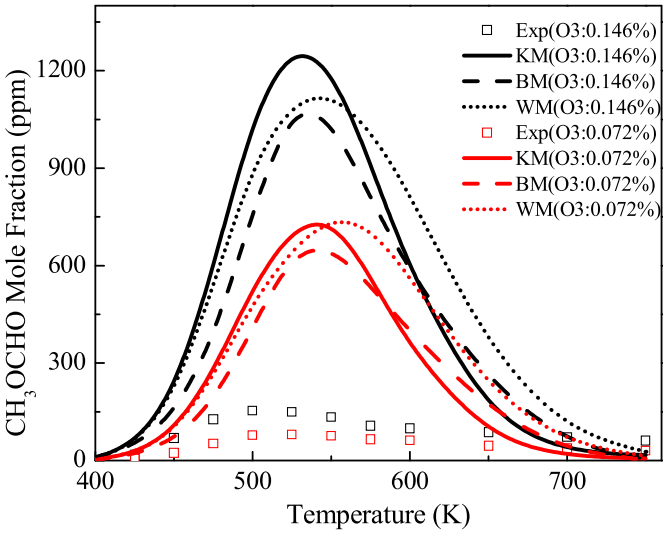

Fig. 8. CH_3OCHO mole fraction profiles with varied temperatures.

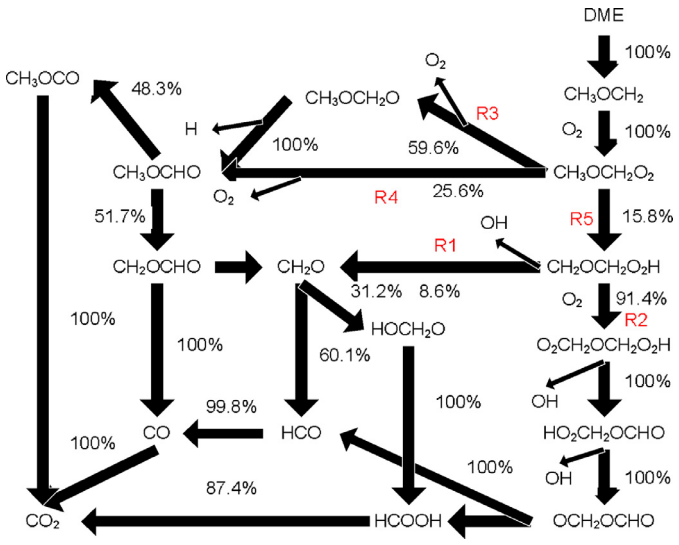

Fig. 7. Reaction path analysis of DME at 500 K (O_3:0.146%).

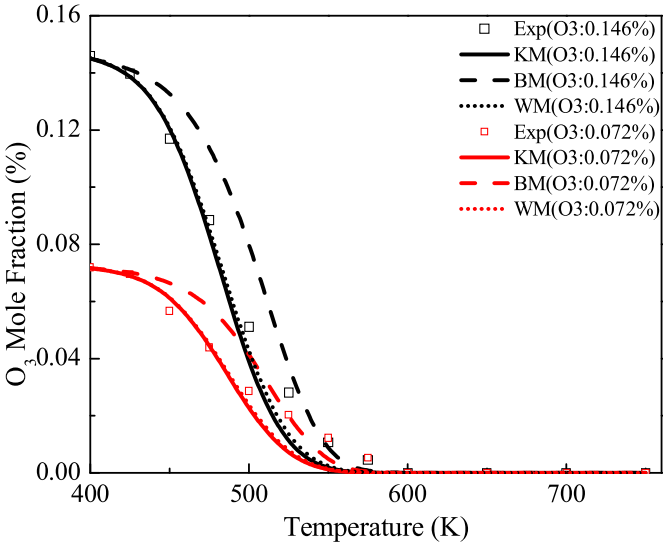

Fig. 9. O_3 mole fraction profiles with varied temperatures.

under-predicted by all models. The opposite direction in predicted DME and O_2 consumptions compared to experimental results suggests that there is a large uncertainty in the reaction pathways for O_2 production or consumption. To understand the detailed mechanism of DME oxidation, a reaction path analysis of DME consumption is performed for case 1 (O_3: 0.146%) at 500 K and shown in Fig. 7. From Fig. 7, O_2 is found to be mainly consumed by the association with CH_3OCH_2 but reproduced through the disassociation reactions of $CH_3OCH_2O_2$, (R_3) and (R_4). (R_3) and (R_4) are the major competing chain-propagation and branching pair for the disassociation reactions of $CH_3OCH_2O_2$.The isomerization of $CH_3OCH_2O_2$ to $CH_2OCH_2O_2H$ via (R_5) is another channel that consumes $CH_3OCH_2O_2$ but does not produce O_2. The branching ratio of $CH_3OCH_2O_2$ is defined as β_2 = net production of O_2 from $CH_3OCH_2O_2$/total consumption of $CH_3OCH_2O_2$.

$$2CH_3OCH_2O_2 = 2CH_3OCH_2O + O_2 \quad (R_3)$$

$$2CH_3OCH_2O_2 = CH_3OCH_2OH + CH_3OCHO + O_2 \quad (R_4)$$

$$CH_3OCH_2O_2 = CH_2OCH_2O_2H \quad (R_5)$$

Note that the higher β_2 is, the more O_2 is regenerated and the more CH_3OCHO is produced. The over-predicted branching ratio of $CH_3OCH_2O_2$ via (R_3) and (R_4) in the kinetic models may explain why the predicted O_2 is too high but the predicted DME is too low.

From Fig. 8, it is clearly seen that CH_3OCHO is significantly over-predicted. As discussed above, a higher branching ratio of β_2 will lead to higher CH_3OCHO and O_2 mole fractions. The over-prediction of CH_3OCHO, together with the over-prediction of O_2, reveals that the branching ratio of $CH_3OCH_2O_2$ decomposition to CH_3OCHO and O_2 may have large uncertainties.

Figure 9 shows the mole fraction of O_3 measured at the exit of the flow reactor at different temperatures. In the experiment, there is nearly no O_3 observed in the mixture above 575 K and above that all the O_3 decompose to O_2 and O radicals. The O_3 sub-mechanism in Kurimoto's model and Wang's model slightly over-predicts the O_3 consumption at higher temperature.

To identify the key reactions affecting the consumption of DME and O_2, sensitivity analyses for DME are performed at 500 K and 600 K using Kurimoto's model (Figs. 10 and 11), respectively. The sensitivity for DME mole fraction is defined as:

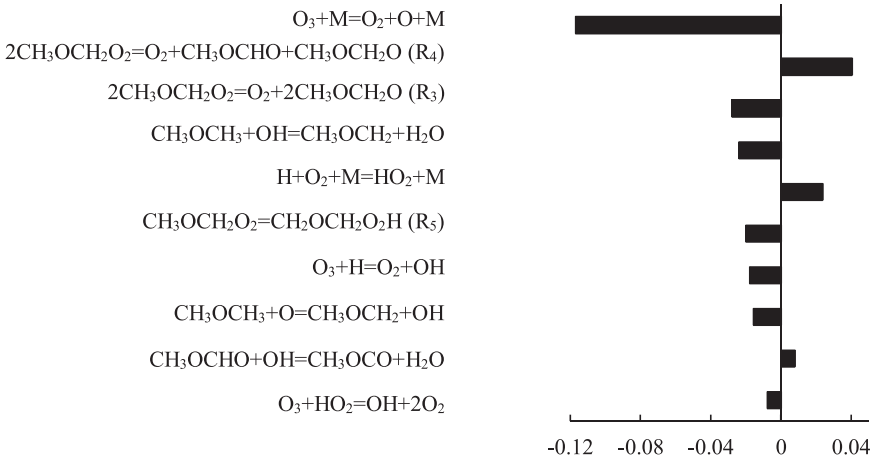

Fig. 10. Normalized sensitivity analysis for DME at 500 K (O_3:0.146%).

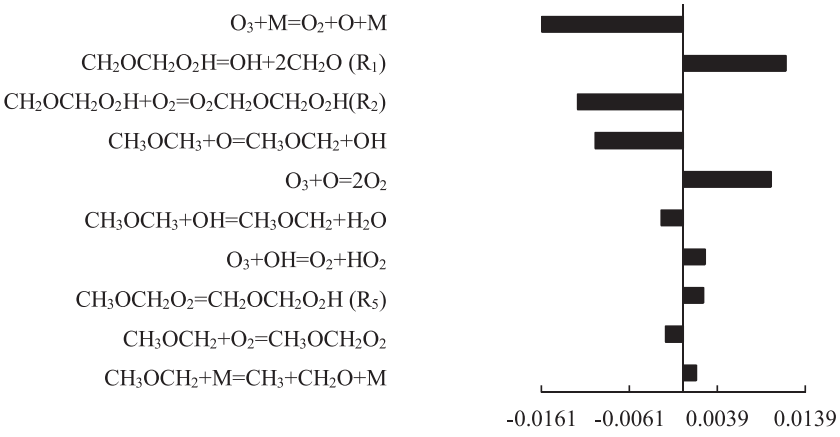

Fig. 11. Normalized sensitivity analysis for DME at 600 K (O_3:0.146%).

Sensitivity$_{DME}$= ($\Delta X_{DME}/X_{DME}/(\Delta k_i/k_i)$), where X_{DME} is the mole fraction of DME, and k_i is the ith reaction's rate constant.

It is seen that O_3 decomposition reaction dominates the low temperature oxidation of DME, and (R_3), (R_4) and (R_5) are also very important pathways to influence the consumption of DME at low temperature (500 K). At higher temperature (above 600 K), the reaction channels via (R_1) and (R_2) tend to be more important.

The mole fraction profiles of CO and CO_2 are summarized in Figs. 12 and 13, respectively. For the experimental data, initially, both of the two species appear once the consumption of DME is observed. Their mole fractions rise with the increase of the reactor temperature and peak around 600 K and 550 K, respectively, and their mole fractions are under-predicted in the model. From the sensitivity analyses of CO and CO_2 at 600 K in Figs. S4 and S5 of the supplementary material, the discrepancy between experiments and models mainly comes from (R_1) to (R_5).

CH_2O is one of the most important intermediate species at low temperature oxidation of DME, and its measured and predicted mole fractions are shown in Fig. 14. Both in the experiments and the model predictions, CH_2O mole fraction rises with increasing temperature and the amounts of O_3 addition have small influence on the CH_2O distribution. From the sensitivity analysis of CH_2O at 600 K in Fig. S3 of the supplementary material, the uncertainty mainly comes from (R_1) and (R_2). Below 600 K, because the reactivity of the system becomes higher with increasing temperature, more intermediate species (e.g. CH_2O, H_2O_2) are produced. At higher temperature (600 K and above), (R_1) is more important than (R_2), causing a further increase of CH_2O formation. It is seen

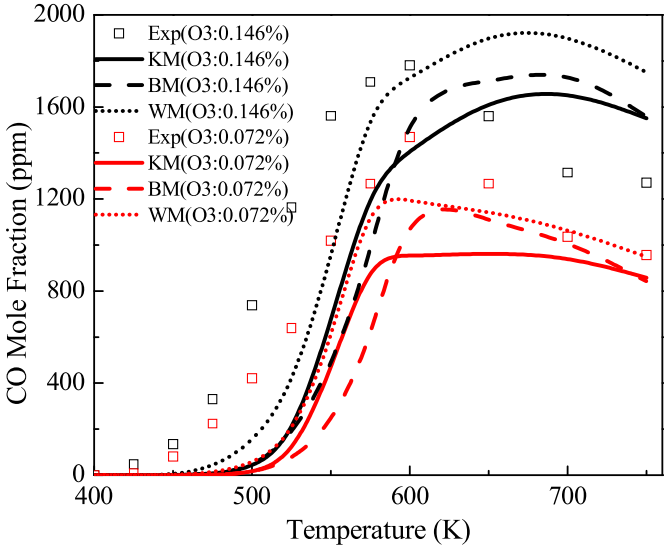

Fig. 12. CO mole fraction profiles with varied temperatures.

that models under-predict CH_2O mole fraction significantly below 575 K, while over-predict the mole fraction with higher temperature. Interestingly, in the existing DME oxidation experiment without ozone, instead of showing a monotonically increasing trend,

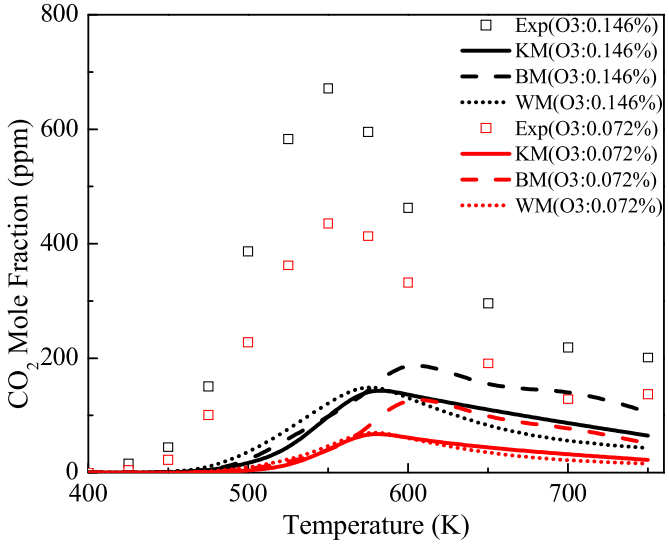

Fig. 13. CO_2 mole fraction profiles with varied temperatures.

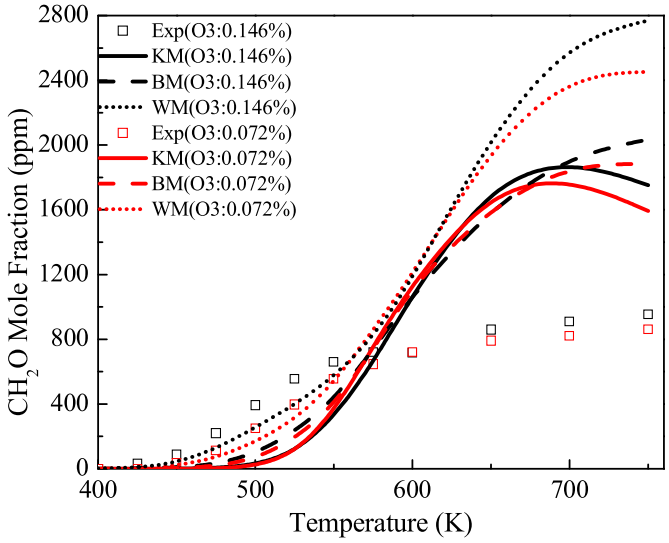

Fig. 14. CH_2O mole fraction profiles with varied temperatures.

CH_2O mole fraction decreases above 650 K. That's because DME consumption reduces above 650 K, causing less formation of CH_2O.

This discrepancy in CH_2O profiles between experiments and models implies possible deficiencies of the kinetic models. (R_1) and (R_2) are the two key reactions in the low temperature chemistry of DME. Below 600 K, as suggested by Kurimoto et al. [4], a higher ratio of β_1 is required to decrease the system reactivity and increase the formation of CH_2O. When the temperature is higher than 600 K, a lower ratio of β_1 is needed to reduce the over-predictions of CH_2O in the models. Therefore, the present experimental results provide a good validation target to validate high level quantum chemistry and kinetics calculation on (R_1) and (R_2). A negative temperature dependent branching ratio of competing chain propagating and branching reaction pairs, (R_1) and (R_2), will help to reduce the uncertainties in the models.

H_2O_2 is another important intermediate species at low temperature, which is quantitatively measured in this experiment and shown in Fig. 15. The models predict the temperature window of H_2O_2 well, but significantly over-predict the peak mole fraction. The over-prediction of H_2O_2 may be due to the high branching ratio of β_2, which over-predicts H radical production and leads to the subsequent formation of HO_2 and H_2O_2. From the sensitivity analysis of H_2O_2 at 600 K in Fig. S6 of the supplementary material, H_2O_2 prediction is affected from both (R_3)–(R_5) competing pair and (R_1)–(R_2) competing pair.

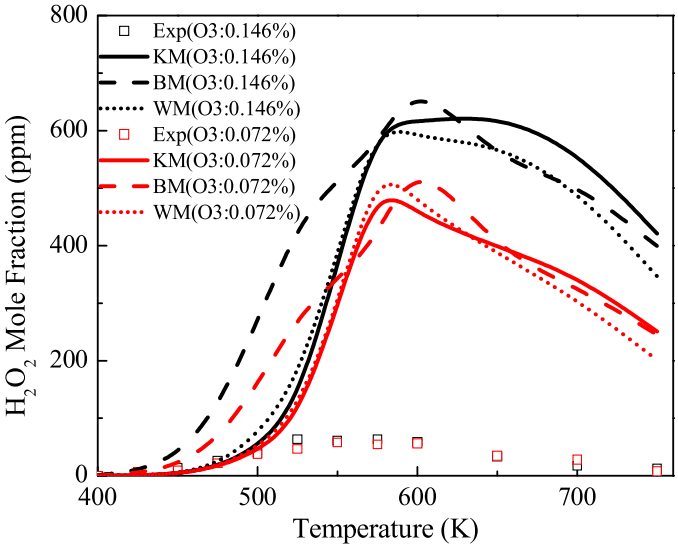

Fig. 15. H_2O_2 mole fraction profiles with varied temperatures.

4. Conclusions

The ozone assisted low temperature oxidation chemistry of DME from 400 K to 750 K was investigated in the mixture of $DME/O_3/O_2/He/Ar$ using an atmospheric-pressure flow reactor coupled with MBMS. By the comparisons between model predictions and experimental results, we have found that,

(1) O_3 addition not only significantly enhances the low temperature oxidation of DME, but also lowers the oxidation temperature window by ~100 K. Therefore, ozone is a good chemical sensitizer to magnify the uncertainty of low temperature chemistry at low temperature. The present results give a good explanation to mechanism of ozone assisted cool flames.

(2) The discrepancies between the model predictions and experimental results around 600 K on DME, CH_2O, CO, CO_2 indicate that branching ratio of the competing chain-propagation and branching reaction pairs, (R_1) and (R_2), need to be further increased in lower temperature but decreased at higher temperature.

(3) The significantly over-predicted O_2 regeneration and CH_3OCHO formation indicate that the branching ratio of another competing chain-propagation and branching reaction pair, involving (R_3) and (R_4), is probably overestimated in these kinetic models.

O_3 decomposition is one of the most important reactions in the low temperature oxidation of DME, and its decomposition and consumption is worth to be further investigated. These experimental results provide a more clearly guide for theoretical predictions of low temperature chemistry reactions and validation targets for reaction mechanism development.

Acknowledgments

This research was partly funded by the NSF Grant CBET-1507358 and the Princeton Andlinger Center for Energy and the Environment (ACEE) grand challenge grant.

Supplementary materials

Supplementary material associated with this article can be found, in the online version, at doi:10.1016/j.combustflame.2016.08.008.

References

[1] T.A. Semelsberger, R.L. Borup, H.L. Greene, Dimethyl ether (DME) as an alternative fuel, J. Power Sources 156 (2006) 497–511.
[2] H. Yamada, M. Yoshii, A. Tezaki, Chemical mechanistic analysis of additive effects in homogeneous charge compression ignition of dimethyl ether, Proc. Combust. Inst. 30 (2005) 2773–2780.
[3] H. Guo, W. Sun, F.M. Haas, T. Farouk, F.L. Dryer, Y. Ju, Measurements of H_2O_2 in low temperature dimethyl ether oxidation, Proc. Combust. Inst. 34 (2013) 573–581.
[4] N. Kurimoto, B. Brumfield, X. Yang, T. Wada, P. Dievart, G. Wysocki, Y. Ju, Quantitative measurements of HO_2/H_2O_2 and intermediate species in low and intermediate temperature oxidation of dimethyl ether, Proc. Combust. Inst. 35 (2015) 457–464.
[5] J. Gao, Y. Nakamura, Low-temperature ignition of dimethyl ether: transition from cool flame to hot flame promoted by decomposition of HPMF (HO_2CH_2OCHO), Combust. Flame 165 (2016) 68–82.
[6] Y. Ju, C.B. Reuter, S.H. Won, Numerical simulations of premixed cool flames of dimethyl ether/oxygen mixtures, Combust. Flame 162 (2015) 3580–3588.
[7] Z. Zhao, M. Chaos, A. Kazakov, F.L. Dryer, Thermal decomposition reaction and a comprehensive kinetic model of dimethyl ether, Int. J. Chem. Kinet. 40 (2008) 1–18.
[8] U. Burke, K.P. Somers, et al., An ignition delay and kinetic modeling study of methane, dimethyl ether, and their mixtures at high pressures, Combust. Flame 162 (2015) 315–330.
[9] S.L. Fischer, F.L. Dryer, H.J. Curran, The reaction kinetics of dimethyl ether. I: high-temperature pyrolysis and oxidation in flow reactors, Int. J. Chem. Kinet. 32 (2000) 713–740.
[10] U. Pfahl, K. Fieweger, G. Adomeit, Self-ignition of diesel-relevant hydrocarbon-air mixtures under engine conditions, Symp. (Int.) Combust. 26 (1996) 781–789.
[11] P. Dagaut, J.C. Boettner, M. Cathonnet, Chemical kinetic study of dimethylether oxidation in a jet stirred reactor from 1 to 10 ATM: experiments and kinetic modeling, Symp. (Int.) Combust. 26 (1996) 627–632.
[12] H.J. Curran, W.J. Pitz, C.K. Westbrook, P. Dagaut, J.-C. Boettner, M. Cathonnet, A wide range modeling study of dimethyl ether oxidation, Int. J. Chem. Kinet. 30 (1998) 229–241.
[13] X. Qin, Y. Ju, Measurements of burning velocities of dimethyl ether and air premixed flames at elevated pressures, Proc. Combust. Inst. 30 (2005) 233–240.
[14] D. Liu, J. Santner, C. Togbé, et al., Flame structure and kinetic studies of carbon dioxide-diluted dimethyl ether flames at reduced and elevated pressures, Combust. Flame 160 (2013) 2654–2668.
[15] K. Moshammer, A.W. Jasper, D.M. Popolan-Vaida, et al., Detection and identification of the keto-hydroperoxide ($HOOCH_2OCHO$) and other intermediates during low-temperature oxidation of dimethyl ether, J. Phys. Chem. A 119 (2015) 7361–7374.
[16] F. Herrmann, P. Oßwald, K. Kohse-Höinghaus, Mass spectrometric investigation of the low-temperature dimethyl ether oxidation in an atmospheric pressure laminar flow reactor, Proc. Combust. Inst. 34 (2013) 771–778.
[17] P. Dagaut, J. Luche, M. Cathonnet, The low temperature oxidation of DME and mutual sensitization of the oxidation of DME and nitric oxide: experimental and detailed kinetic modeling, Combust. Sci. Technol. 165 (2001) 61–84.
[18] W. Sun, S.H. Won, Y. Ju, In situ plasma activated low temperature chemistry and the S-curve transition in DME/oxygen/helium mixture, Combust. Flame 161 (2014) 2054–2063.
[19] T. Ombrello, S.H. Won, Y. Ju, S. Williams, Flame propagation enhancement by plasma excitation of oxygen. Part I: effects of O_3, Combust. Flame 157 (2010) 1906–1915.
[20] L.T. Molina, M.J. Molina, Absolute absorption cross sections of ozone in the 185-to 350-nm wavelength range, J. Geophys. Res. 91 (1986) 14501–14308.
[21] Z. Wang, X. Zhang, L. Xing, L. Zhang, F. Herrmann, K. Moshammer, F. Qi, K. Kohse-Höinghaus, Experimental and kinetic modeling study of the low-and intermediate-temperature oxidation of dimethyl ether, Combust. Flame 162 (2015) 1113–1125.
[22] F.L. Dryer, F.M. Haas, J. Santner, et al., Interpreting chemical kinetics from complex reaction–advection–diffusion systems: modeling of flow reactors and related experiments, Prog. Energy Combust. Sci. 44 (2014) 19–39.
[23] http://www.reactiondesign.com/products/chemkin/chemkin-pro/ (accessed 04.08.13).
[24] W.M. Jones, et al., The thermal decomposition of ozone in a shock tube, J. Am. Chem. Soc. 84 (1962) 2868–2878.
[25] C.C. Schubert, R.N. Pease, The oxidation of lower paraffin hydrocarbons. I. Room temperature reaction of methane, propane, n-butane and isobutane with ozonized oxygen, J. Am. Chem. Soc. 78 (1956) 2044–2048.
[26] R.J. Morrissey, C.C. Schubert, The reactions of ozone with propane and ethane, Combust. Flame 7 (1963) 263–268.
[27] J.B. Pedley, Thermochemical data of organic compounds, 2nd ed., Chapman and Hall, London, 1986.
[28] S.J. Blanksby, G.B. Ellison, Bond dissociation energies of organic molecules, Acc. Chem. Res. 36 (2003) 255–263.